S. BAGCHI
P. PREM KIRAN
M.K. BHUYAN
S. BOSE
P. AYYUB
M. KRISHNAMURTHY
G.R. KUMAR[✉]

Fast ion beams from intense, femtosecond laser irradiated nanostructured surfaces

Tata Institute of Fundamental Research, 1 Homi Bhabha Road, Colaba, Mumbai 400005, India

ABSTRACT We present results on hot electron and energetic ion (keV–MeV) generation from polished and nanostructured metallic surfaces excited by p-polarized, femtosecond laser pulses in the intensity range of 1×10^{15}–1.5×10^{17} W cm^{-2}. A clear enhancement in the hard X-ray spectrum from nanoparticle-coated surfaces is observed, indicating 'hotter' electron production in nanoparticle-produced plasma until the intensity of 2×10^{16} W cm^{-2} is reached. Contrary to the existing perception, we find that the hotter electrons do not lead to hotter ion emission. The total ion flux and the ion energy integrated over the 4–1400 keV energy range are found to be enhanced by 50% and 16%, respectively, for nanostructured targets in comparison to those from polished targets. 55% enhancement in yield is observed for ions at the lower end of the energy range, while hotter ions are actually found to be suppressed by $\sim 40\%$. The surface modulations present on the nanoparticle-coated targets are observed to reduce the maximum energy of the ions and showed an intensity-dependent increase in the divergence of the ion beam.

PACS 79.20.Ds; 68.47.De; 61.80.Ba; 61.82.Bg; 42.65.Re

1 Introduction

The interaction of intense, ultra-short, femtosecond laser pulses with matter leads to the production of hot plasma, a rich source of hard X-rays, 'hot' electrons and fast ions. Huge electromagnetic fields induced by the laser pulse in the plasma can accelerate electrons and ions to produce collimated beams of bright and high-energy particles [1–5]. The ability to generate high accelerating fields, particle currents and current densities of ultra-short duration from these compact laser-driven particle beams has potential applications in various domains of science, technology and medicine [6–9]. When an intense laser pulse interacts with the target, rapid ionization occurs at the beginning of the laser pulse and the electrons in the plasma then absorb the light by a variety of collisional as well as collisionless mechanisms like resonance absorption (RA), vacuum heating (VH), etc. [10, 11]. The electrons which gain energy through these mechanisms form a distinct 'hot' bunch well separated in energy from the

[✉] Fax: +91-22-2280-4610, E-mail: grk@tifr.res.in

colder electrons in the bulk plasma. Ion acceleration occurs when the hot plasma expands and an electric field is created due to charge separation. Ion acceleration in plasma with multiple electron temperatures has been explored in different experimental situations and also in extensive numerical simulations [12–15].

Efficient coupling of laser energy into the short-lived plasma plays a crucial role in 'hot' electron generation. Enhanced coupling of laser energy to the plasma has been achieved by the creation of a preplasma before the arrival of the main pulse, by modifying target composition in the case of clusters [16] or microdroplets [17] and by the introduction of sub-laser-wavelength surface modulations on solid targets [18–21]. Surface modulations can give as much as 80% coupling of laser energy, leading to generation of 'hotter' electrons manifested in terms of 'harder' X-rays. Based on the existing understanding of ion emission processes that hotter electrons should lead to hotter ions [2–5, 13, 14], in this paper we address a very important question – can ion energies be similarly increased by similar optimization of the target properties? We present a systematic study of the influence of the surface modulations created by nanoparticle coating on a metal surface on the characteristics of the keV hard X-rays and ions in the keV–MeV energy range from a femtosecond laser produced plasma.

2 Experimental arrangement: X-ray and ion diagnostics

The schematic of the experimental setup is shown in Fig. 1. The experimental chamber is pumped by a turbo molecular pump (Varian V-301, 250 l/s) supported by a dry pump (Alcatel 610 l/s). The base pressure of the chamber is close to 10^{-8} Torr. The motorized x–y–θ–z stage assembly, where z is the laser propagation direction and θ is the rotation angle about the y (vertical) axis, enables the scanning of the target across the laser beam, so that the laser pulse always hits a fresh target region. It can also move the target across the laser focus to adjust the focal spot intensity at fixed laser energy. The target is a polished copper block ($50 \times 50 \times 5$ mm), half of which is coated with a 0.3-μm layer of ellipsoidal copper nanoparticles (CuNP) with an average size of 15 nm and an aspect ratio of 1.5. The nanoparticles are deposited using a high-pressure dc magnetron sputtering technique [22]. The crystallite size
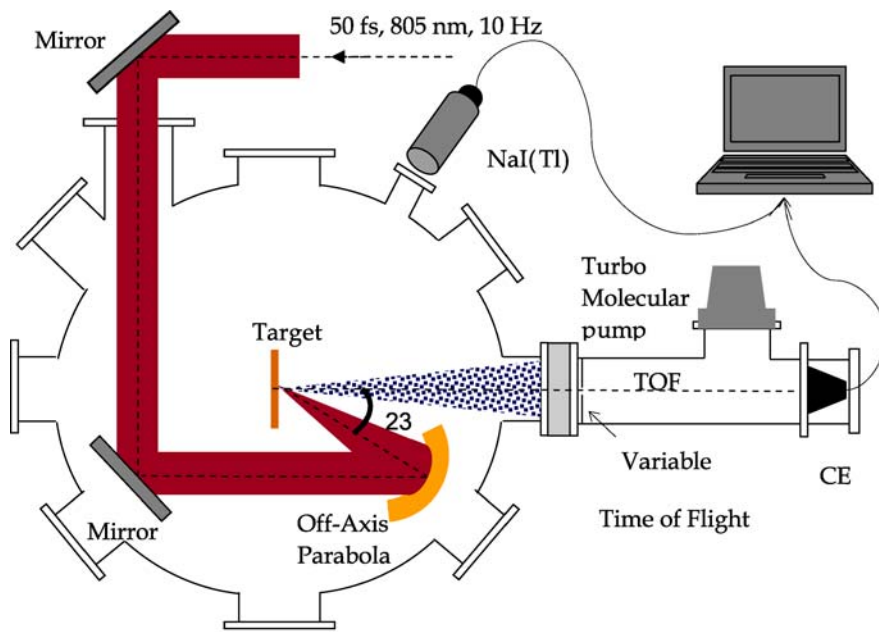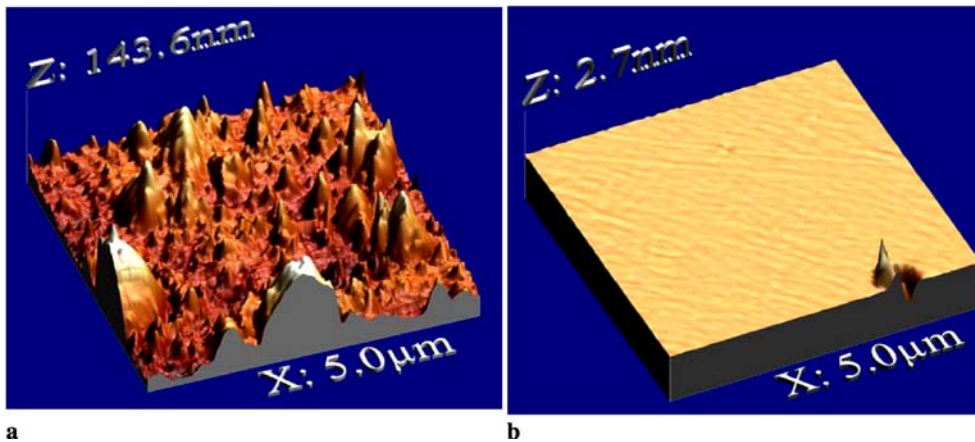
FIGURE 1 Schematic diagram of the experimental setup. The *insets* show the processed AFM images of (**a**) a CuNP-coated surface and (**b**) a polished Cu surface. The big humps in the AFM pictures correspond to clusters of nanoparticles. The average size of the nanoparticles is determined from X-ray diffraction techniques and found to be 15 ± 2 nm

a   b

is determined from the Scherrer broadening of the Cu [111] X-ray diffraction line. The areal density of the nanoparticles is close to 30% of the solid density. The partially coated target ensures exactly the same laser and detector conditions for measurements from the coated and uncoated portions of the surface.

The targets are irradiated with focused 50-fs, p-polarized laser pulses from a 806-nm, 10-Hz, Ti:sapphire laser (Thales Laser, Alpha 10) with a contrast ratio of $10^6 : 1$ for the fs to the ns pedestal. The laser is focused on to the target by a gold-coated off-axis parabolic mirror (OAP), in an $f/4$ focusing geometry at $23°$ with respect to the target normal. The focal spot size (FWHM) measured by the equivalent imaging method is $10\,\mu m$, giving a peak intensity of 1×10^{15}–$1.5 \times 10^{17}\,\mathrm{W\,cm^{-2}}$. Throughout the measurement the laser fluctuations were ensured to be within 5%. With all the components inside, the base pressure inside the vacuum chamber is $\sim 10^{-6}$ Torr. The time of flight (TOF) assembly is differentially pumped in order to keep the channel electron multiplier (CEM) at a steady pressure of 10^{-7} Torr for its proper operation without any damage due to unwanted avalanche processes.

The hard X-ray spectra in the 20–200 keV range are measured for a total of 3000–4000 laser shots using a NaI(Tl) scintillation detector kept in the plane of incidence at $45°$ to the target normal. It is shielded by 1-cm-thick lead bricks to eliminate stray radiation and calibrated using a Cs^{137} radioactive source. The detector is gated in time with the laser pulse and the signal is collected in a time window of $30\,\mu s$, to ensure nearly background-free acquisition. The signal from the detector was amplified and then fed to a multichannel analyzer through an analog to digital converter. The BK-7 window of the vacuum chamber sets a low-energy cutoff at about 12 keV for the observed emission and the bremsstrahlung temperature fits presented are done using the data above 50 keV, where the transmission is close to 100%. The X-ray count rate is kept less than 0.1 per laser shot by proper detector positioning and placing suitable lead apertures in front of the detector. This was necessary to prevent radiation pile up.

The energy spectrum of the ions emitted normal to the target surface was measured using a conventional ion time of flight technique, with a channel electron multiplier placed at a distance of 97 cm from the laser focus. The solid angle for ion collection was 26 msr. The arrival times of the charged

particles at the detector were recorded with a 1-GHz digital storage oscilloscope. A large-area Faraday cup (FC) (230 cm^2), placed at a distance of 35 cm from the target surface, was used to collect all the emitted charged particles from the plasma in order to obtain the total ion flux. The FC, made of 11-µm-thick aluminium foil, was biased at -300 V. A nickel mesh was placed in front of the FC biased at a voltage of -500 V to repel the secondary electrons. It is to be noted that the FC stops all the heavier ions, while transmitting higher-energy electrons [23, 24].

3 Results

The bremsstrahlung (hard X-ray) spectra from both the polished Cu and the CuNP-coated surfaces at the input intensity of 3×10^{16} W cm^{-2} are shown in Fig. 2. The hot electron distribution in a Cu plasma is a single Maxwellian with a temperature of 9.3 ± 1.1 keV, whereas the CuNP plasma shows a bi-Maxwellian electron distribution with temperatures 9.5 ± 1.7 keV and 33.9 ± 6.4 keV, indicating the presence of hotter electrons in the plasma due to the enhanced coupling of laser energy into the NP-coated surface via surface plasmons when compared to the polished surface [18–20]. The integrated energy of X-rays emitted in the range of 30–200 keV for polished Cu and NP surfaces is 2.9×10^{-9} mJ and 7.05×10^{-9} mJ, respectively. The ratio of total X-ray yield from a CuNP-coated surface to that from the polished Cu surface at different input laser energies corresponding to the intensities in the range of 0.9–3.6×10^{16} W cm^{-2} is shown as the inset in Fig. 2. At a lower intensity the bremsstrahlung yield from nanoparticles is four times larger than that of the polished surface. With the increase in intensity the yield relatively decreases, but even at the highest intensity (3.6×10^{16} W cm^{-2}) used in the experiment the yield from a nanoparticle-coated surface is around 50% higher than the
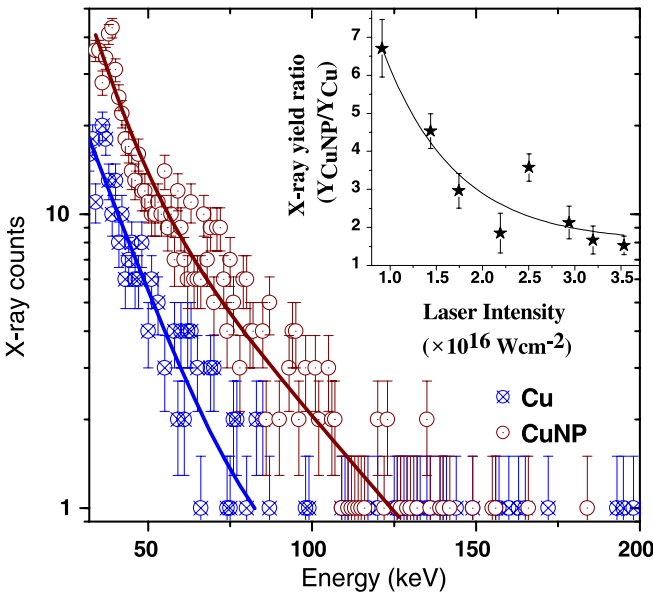
polished surface. We discuss the reason for this decrease later in the paper.

Under our experimental conditions, the hot electrons are generated mainly by RA [10, 11]. The hot electron temperature, T_{hot}, can be estimated [25] as $T_{hot} = 14 T_c^{0.33} (I\lambda^2)^{0.33}$, where T_c is the background electron temperature in keV, I the laser intensity in 10^{16} W cm^{-2} and λ the wavelength in µm. For a T_c of 150 eV (estimated for our intensities), we obtain a T_{hot} of 9.2 keV. This temperature is close to that observed for the polished target and the lower of the two components observed in the nanoparticle-coated targets and agrees with earlier measurements [18–20, 28]. The hotter component of 33.9 keV is attributed to local field enhancements of the laser light or alternately surface plasmon excitation facilitated by the nanoparticle coating [18–21].

Figure 3 shows $n(E)$–E spectra of ions generated from Cu (solid lines) and CuNP (dashed lines), where $n(E)$ is the number of ions emitted within the energy range of E to $E + \mathrm{d}E$ at three different input intensities with corresponding time of
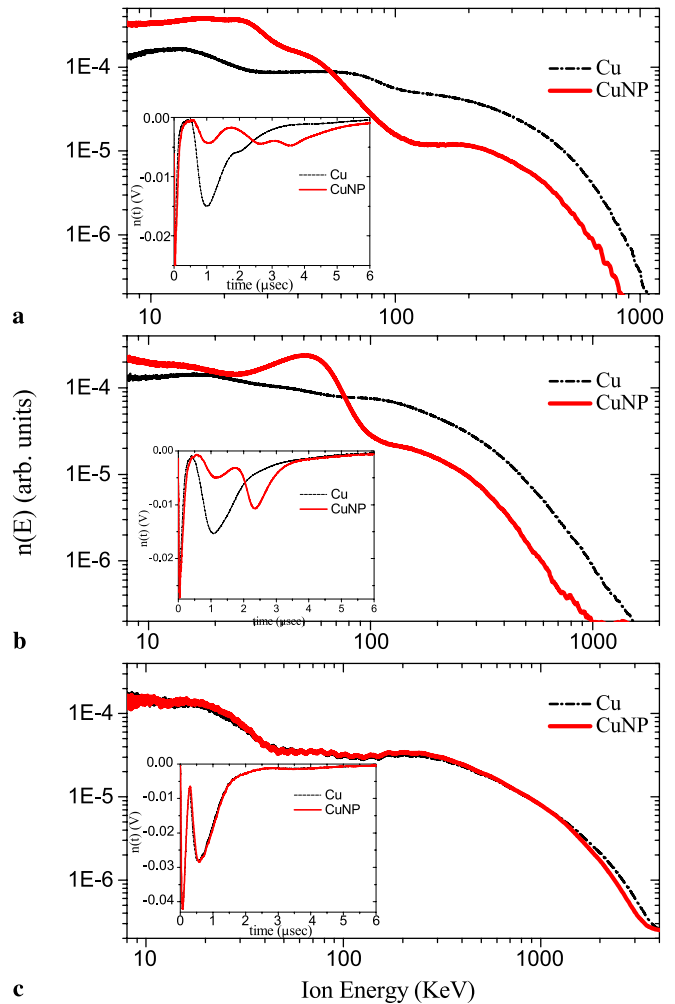

FIGURE 3 $n(E)$–E spectra of ions emitted from CuNP (*solid red*) and Cu (*dashed black*) surfaces at input laser intensities of (**a**) 0.9×10^{16}, (**b**) 3.5×10^{16} and (**c**) 1×10^{17} W cm^{-2}, respectively. The *insets* show the TOF spectra of polished Cu and CuNP. It is clearly seen that the CuNP TOF spectra always consist of multiple ion distributions except at the highest laser energy. The protons are found on zooming on to the TOF spectra. The proton population is found to be of the same order in both cases

FIGURE 2 Bremsstrahlung spectra from polished Cu and CuNP on polished copper at a laser intensity of 3×10^{16} W cm^{-2}. The *inset* shows the ratio of total X-ray yield from the CuNP and Cu surfaces with laser energy. The *line* in the *inset figure* is a guide for the eye

flight spectra as insets. Both the $n(E)$–E and the TOF spectra clearly show the differences in energies observed from the polished Cu and NP-coated surfaces. At a lower input intensity of 0.9×10^{16} W cm^{-2}, the polished Cu surface shows two main features representing two different ion species around 65 ± 15 and 240 ± 25 keV energy, while the CuNP surface gives three distinct peaks with energies of 25 ± 10, 45 ± 10 and 320 ± 20 keV (Fig. 3a). On increasing the input intensity to 3.5×10^{16} W cm^{-2}, the two peaks for Cu merge, giving a single distribution of the ions in the 280 ± 60 keV energy range. In contrast, for CuNP, the three-energy distribution evolves into a two-peak feature indicating the presence of two sets of ions of energies 54 ± 8 and 280 ± 40 keV. Above the intensity of 4×10^{16} W cm^{-2} the ion energy spectrum from CuNP starts showing a single peak similar to that of Cu with almost the same energy distribution (Fig. 3c at an intensity of 1×10^{17} W cm^{-2}). This indicates that the nanoparticle coating becomes damaged at the higher intensity, an observation in agreement with our earlier studies [29].

Below an intensity of 4×10^{16} W cm^{-2}, where the NP coating remains intact, the ion energy spectra from Cu and CuNP show an interesting feature. The total ion flux ($\int n(E)\mathrm{d}E$) from the NP-coated surface is higher than that from the Cu in the 4–75 keV ion energy range (region A) compared to the flux in the 75–1400 keV range (region B) (Fig. 4a), while in the 4–1400 keV range the ion flux from the NP surface is higher by 55%. Similarly, the total ion energy ($\int En(E)\mathrm{d}E$) in the 4–75 keV range has increased by 52% for CuNP surfaces compared to Cu surfaces, while in the 75–1400 keV range they have reduced by 60%. Also, in the total range of 4–1400 keV ion energy, the total ion flux and the ion energy in the full energy range are larger by 50% and 16%, respectively, from CuNP targets compared to Cu targets (Fig. 4b). The mean ion energy (ratio of total ion energy to the number of particles; $\int En(E)\mathrm{d}E/ \int n(E)\mathrm{d}E$) from the CuNP surface has increased by $5(\pm 0.5)\%$ in the low-energy range and has reduced by $10(\pm 1.0)\%$ in the high-energy range, compared to that from the polished Cu surface. While the total ion energy in the entire energy range increases by 16%, the mean ion energy reduces by 20%, due to the enhanced flux of low-energy ions.

Figure 5 shows the variation of the maximum energy per ion ($E_{\max}$) with $I\lambda^2$ (Wcm^{-2} μm^2) for both types of target, in the intensity range 2×10^{15}–1×10^{17} W cm^{-2} μm^2. The maximum ion energy from the Cu plasma increases from 0.6 to 3.6 MeV with increasing laser intensity. In the intensity range of 2×10^{15}–3.5×10^{16} W cm^{-2} μm^2, the maximum ion energies from the CuNP surface range between 0.5 and 2.0 MeV indicating a reduction of around 18% in the energetic ion emission from the CuNP plasma. The maximum ion energy ($E_{\max}$) measured in the sub-relativistic-intensity regime can be estimated from the hot electron temperatures using the scaling established by Clark et al. [15] and Zhidkov et al. [13]. For self-similar plasma expansion the maximum ion energy is theoretically estimated to follow $E_{\max} \propto T_{\mathrm{h}} \propto (I\lambda^2)^{0.33-0.5}$. On the other hand, experiments in the intensity regime of 10^{15}–10^{17} W cm^{-2} lead to a scaling of $E_{\max} \propto (I\lambda^2)^{0.4}$. The observed $E_{\max}$ from Cu and CuNP plasmas scale as $(I\lambda^2)^{0.4}$, in agreement with these earlier reports [13, 15]. Above the input intensity of 3.2×10^{16} W cm^{-2}, $E_{\max}$ from CuNP sur-
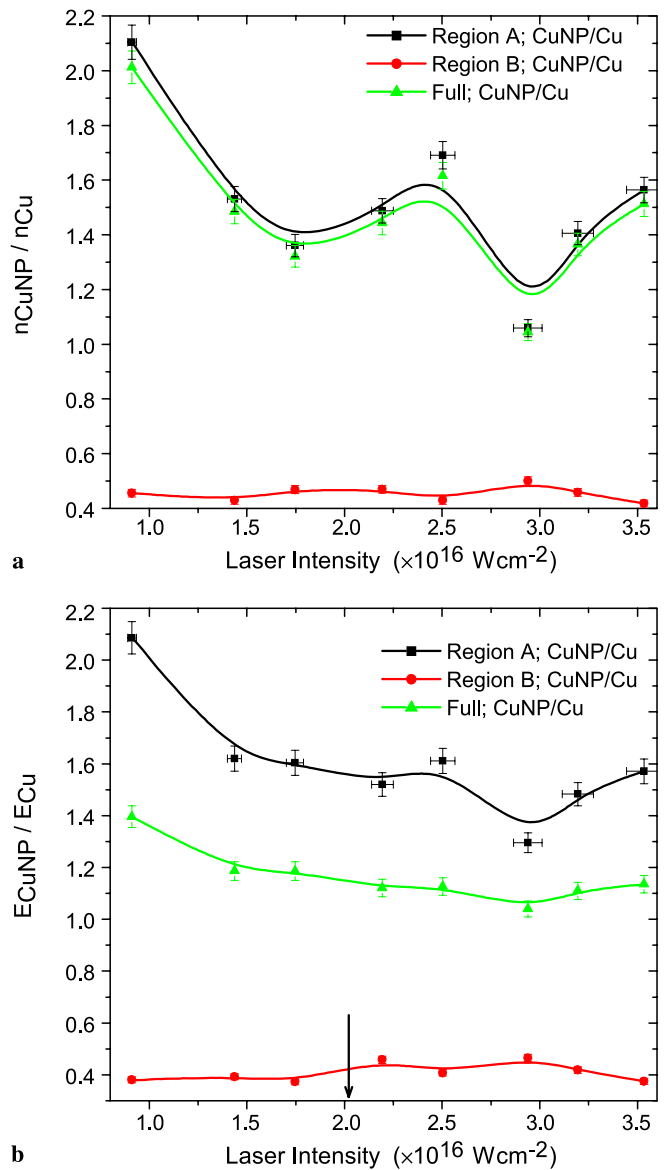
a

b

FIGURE 4   Ratio of (**a**) total ion flux and (**b**) total ion energy from CuNP to polished Cu in 4–75 keV (region A), 75–1400 keV (region B) and over 4–1400 keV (full) energy ranges as a function of input laser intensity. The *down arrow* on the *x* axis represents the laser intensity until which the nanoparticles definitely survive (see text for details). *Lines* in the figure are guides for the eye

faces start approaching that from the Cu surface and above an intensity of 4×10^{16} W cm^{-2}, the cutoff ion energy from the CuNP plasma is almost the same as that for Cu. This indicates damage to the NP coating, in agreement with our previous results [29]. The $E_{\max}$ are observed to be lower than the corresponding values from a polished surface up to an intensity of 3.8×10^{16} W cm^{-2}.

It is clear that more laser energy is coupled to hot electrons in the case of the NP-coated surface. This excess energy, however, does not become transferred to ions. Ion emission from the NP-coated surface becomes preferentially enhanced in the low-energy regime and the highest ion energy actually decreases for the NP-coated surface. This is in contradiction to the usual expectation that the generation of hotter electrons should lead to hotter ion emission [12, 13].
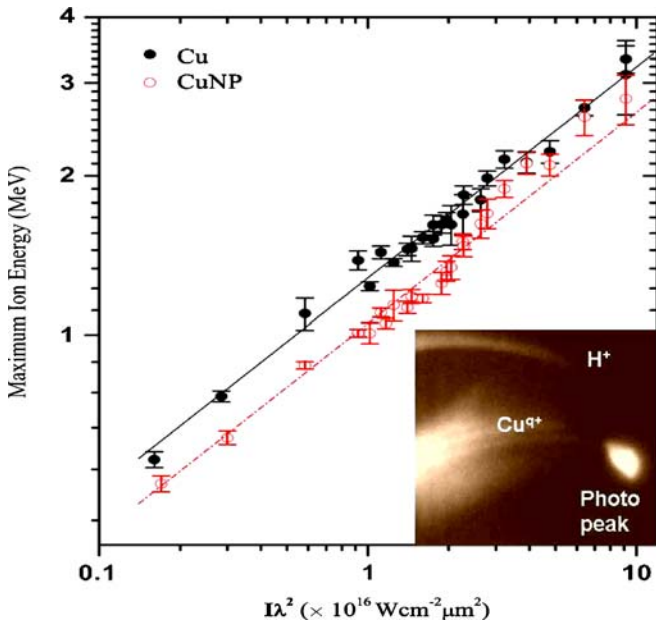
FIGURE 5 Maximum ion energies (per ion) measured from Cu (*solid circles*) and CuNP (*open circles*) as a function of input laser intensity for p-polarized pulses. The *solid black line* shows the scaling of maximum ion energy following $(I\lambda^2)^{0.4}$. The *inset* shows the initial result of the charge-resolved spectra. More experiments are in progress
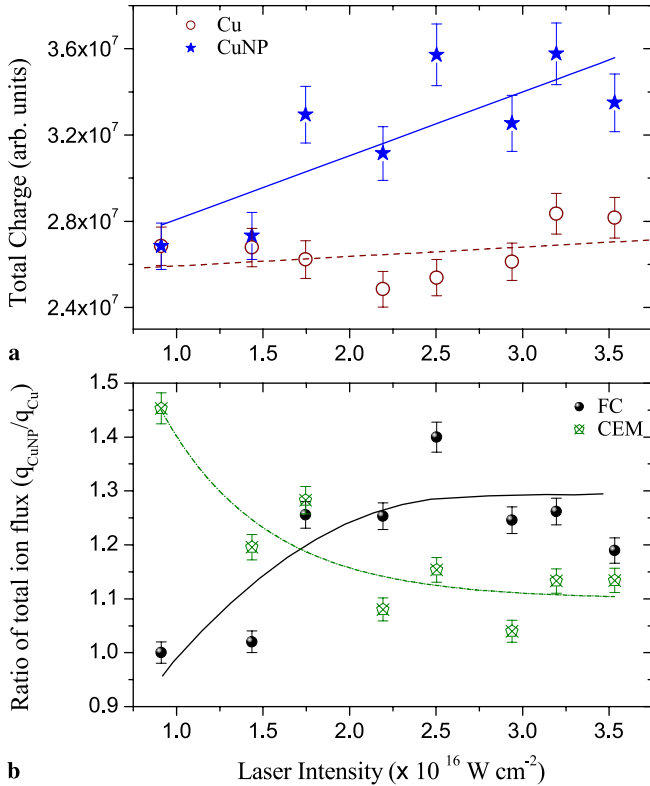

FIGURE 6 (**a**) Total charge accumulated by FC from Cu and CuNP plasma; (**b**) ratio of total ion flux collected using CEM and FC as a function of input laser intensity. *Lines* in the figure are guides for the eye

To obtain a measure of the overall ion yield, we measured the total ion currents from the two types of target at a location much closer to the target, using a large-area Faraday cup (FC) subtending a solid angle of 2.36 Sr to the plasma focus.

Figure 6a shows the total charge present in the plasma accumulated by the FC from Cu and CuNP surfaces. The ratio of the total ion flux from the CuNP to the Cu surface reduces from 45% to 10% as measured by the CEM with increasing laser input intensity, while the flux measured using the FC increases to almost 40% in the case of CuNP targets compared to polished Cu targets (Fig. 6b). The ion yields collected far from the plasma (by the CEM) are anticorrelated with the yields measured close to the target using a FC. The increase in the ratio of the FC signals (q_{CuNP}/q_{Cu}) in contrast to that from the CEM points towards the increasing divergence of the ion emission with increasing laser intensity.

4 Discussion

To understand our experimental observations, first consider the ion emission from a smooth/unstructured (polished Cu) surface. The hot electrons produced by the intense laser, together with the colder electrons, form a two-temperature plasma. The two-temperature plasma gives rise to a sheath formation at a point in the density profile across which the ions are accelerated and these emerge as the hot ions [12]. The field developed across the sheath is $E_{accl} = k_B T_e/e$ [max (L_n, λ_D)], where L_n is the local scale length of the expanding plasma and λ_D is the Debye length [2–5]. The model assumes isothermal expansion which may not be strictly valid, but the general features are well reproduced even under this approximation. As per existing belief [12, 13, 15], hotter electrons produced from the nanoparticle-coated targets should lead to more energetic ions. Our observations are contrary to this. Let us revisit the observed reduction in the maximum ion energies as measured by the TOF technique and the increase in the ion flux measured by the large-area FC closer to the target. What can be the possible reasons for these? One can argue that the protons generated from the NP target could be preferentially enhanced in their energy and the heavier copper ions are therefore unable to benefit from the increased hot electron temperature. From the TOF spectra we found that the protons are not enhanced. The proton energy distributions as well as the yields obtained from both surfaces by high-resolution TOF spectra are very similar and this rules out a difference in proton emission as the cause for the decrease in the energy of Cu^{q+} from nanostructured surfaces. Another possibility of diminishing ion energy from the nanostructured surfaces may be due to the role of inherent laser prepulses originating in the process of pulse amplification. It is known from the experimental studies that the prepulses can influence the plasma properties in a way that diminishes ion energies [32–34]. But, in this experiment it is ensured that the prepulse is 10^{-6} times weaker than the main laser pulse. As the maximum laser intensity of the main pulse used is about 10^{17} W cm^{-2}, the prepulse intensity will be too small to make an impact on the nanostructures, ensuring that the main laser pulse actually interacts with the undistorted structured surface. The third explanation is that the electrostatic sheath responsible for accelerating the ions is severely disturbed due to the enhanced local fields generated by NP-coated surfaces, leading to a divergent ion beam. This argument is worth more exploration, as indicated below.

Firstly, the nanoparticle coating causes significant deviation from the assumption of planar ($\sim$ 1D) expansion, clearly evident in our Faraday cup measurements of the divergence (the nanoparticles are 'smearing out' the ions). It is well known that in multidimensional expansion the maximum energy is lower than that in the one-dimensional (1D) case [35]. It is well known from the experimental and theoretical investigations that surface modulations greatly enhance the surface enhanced Raman scattering (SERS), second-harmonic generation and electron production from solid and cluster targets [16, 18–21]. For an individual ellipsoid the geometrical enhancement factor commonly called the 'lightning rod' factor L_R can be expressed as $L_R = 1 - \xi Q'(\xi)/Q(\xi)$, where $\xi = [1 - (b/a)]^{-1/2}$ and $Q(\xi) = (\xi/2) \ln[(\xi - 1)/(\xi + 1)] - 1$. The parameters '$a$' and '$b$' are the major and minor axes of the ellipsoid. Because of this geometric factor the electric field in the vicinity of the voids is largely enhanced and therefore produces a layer of preplasma in the case of nanostructured surfaces compared to polished surfaces. Thus, the nanoparticles act as the first sources of the plasma because of the enhanced laser intensities in the immediate vicinity of each particle. The plasma is likely to expand away from these hot nanospots with significant nonplanarity, guided mainly by the initial shape of these ellipsoidal particles and these can prevent charge build up and disturb sheath formation resulting in lower sheath voltage and hence lower ion energy. If we take the critical plasma density (10^{21} cm^{-3}) and $T_h = 9.3$ keV, the Debye length is 17 nm, which is the same size as the nanoparticles. The actual Debye length for colder temperatures achieved on the rising edge of the laser pulse is much smaller. The effective Debye length is thus larger and leads to reduced electric fields. It is well known that the basic requirement for RA to occur is the presence of a component of the incident electromagnetic field along the plasma density gradient at a proper scale length [10, 11]. We believe that the modulated plasma density profile originated because the nanostructuring makes coupling of laser to plasma more conducive by providing the appropriate scale length [26, 27] and hence produces hotter plasma. Numerical simulations and experiments show that particle emission occurs normal to the surface and hence nonplanar plasma expansion thus gives rise to increased beam divergence. Divergent ion and proton beams from laser-produced plasmas due to the increased scale length caused by surface modulations have been observed [36, 37]. All these arguments are supported by our recent observations of the survival [29] of these nanoparticles at intensities as high as 2×10^{16} W cm^{-2}. We are in the process of investigating the reduction in the maximum ion energy as well as multispecies ion acceleration using two-dimensional particle-in-cell (PIC) simulations [30, 31], to obtain a better idea of the plasma expansion from the nanoparticle-coated surface.

The present study is significant because it shows that hot electron generation need not cause hotter ion emission. We point out that, in general, optimization of each signal from the plasma requires an understanding of the actual dynamics of the process. In our case, hot electron generation is enhanced by the local field enhancements which increase the effective light intensity. This process takes place on the time scale of the laser pulse (tens of fs). The ion acceleration, however, depends on a subsequent process, namely the plasma expansion and

energy exchange. We believe that this is significantly modified by the same nanoparticles in a counteracting manner and leads to an enhanced number of ions in the low-energy range until 75 keV and reduces the high-energy ions above 75 keV. The reduction in high energy ion emission coupled with enhancement of X-ray emission is very promising for moving towards debris-free and high-brightness hard X-ray sources [38].

5   Conclusion

In summary, we have reported the role of surface modulations in the energetic ion emission from ultra-short intense laser produced plasmas. This study clearly points out that though the surface modulations considerably enhance the coupling of laser energy into the plasma, they do not necessarily lead to emission of 'hotter' ions; a result in contradiction with current wisdom. The difference in flux measurements near to and far away from the target indicates increased angular spread in ion emission from nanoparticle-coated targets. This indicates the complications involved in 'sheath' layer formation as well as ion acceleration. It is important to understand the underlying physics through more experiments and numerical simulations [39]. For a more detailed analysis of the ion acceleration from the nanostructured targets, over and above the conclusions made in this study, it would be important to measure the charge-resolved spectrum. The initial results of the charge-resolved measurement are shown in the inset of Fig. 5. Even in this low resolution the proton trace is clearly visible and a few of the charged states of copper labeled as Cu^{q+} ions are also identifiable. We are carrying out further experiments to improve the experimental resolution with the aim of obtaining charge state resolved studies under varying surface modulations and laser conditions.

REFERENCES

1 B.M. Hegelich, B.J. Albright, J. Cobble, K. Flippo, S. Letzring, M. Paffett, H. Ruhl, J. Schreiber, K. Schulze, J.C. Fernandez, Nature **439**, 441 (2006)
2 S.C. Wilks, A.B. Langdon, T.E. Cowan, M. Roth, M. Singh, S. Hatchett, M.H. Key, D. Pennington, A. MacKinnon, R.A. Snavely, Phys. Plasmas **8**, 542 (2001)
3 V. Malka, Laser Part. Beams **20**, 217 (2002)
4 J. Badziac, A.A. Kozlov, J. Makowski, P. Parys, L. Ryc, J. Wolowski, E. Woryna, A.B. Vankov, Laser Part. Beams **17**, 323 (1999)
5 K. Nemoto, A. Maksimchuk, S. Banerjee, K. Flippo, G. Mourou, D. Umstadter, V.Y. Bychenkov, Appl. Phys. Lett. **78**, 595 (2001)
6 E. Lefebvre, E. d'Humieres, S. Fritzler, V. Malka, J. Appl. Phys. **100**, 113 308 (2006)
7 S. Fritzler, V. Malka, G. Grillon, J.P. Rousseau, F. Burgy, E. Lefebvre, E. d'Humières, P. McKenna, K.W.D. Ledingham, Appl. Phys. Lett. **83**, 3039 (2003)
8 Y. Glinec, J. Faure, J. Fuchs, H. Szymanowski, U. Oelfke, V. Malka, Med. Phys. **33**, 155 (2006)
9 F.V. Hartemann, D. Gibson, W.J. Brown, A. Rousse, K. Ta Phuoc, V. Malka, J. Faure, A. Pukhov, Phys. Rev. ST Accel. Beams **10**, 11 301 (2007)
10 W.L. Kruer, *The Physics of Laser Plasma Interactions* (Addison-Wesley, New York, 1988)
11 F. Brunel, Phys. Rev. Lett. **59**, 52 (1987)
12 J.M. Wickens, J.E. Allen, P.T. Rumsby, Phys. Rev. Lett. **41**, 243 (1978)
13 A. Zhidkov, A. Sasaki, T. Tajima, Phys. Rev. E **61**, 2224 (2000)
14 P. Mora, Phys. Rev. Lett. **90**, 185 002 (2003)
15 E.L. Clark, K. Krushelnick, M. Zepf, F.N. Beg, M. Tatarakis, A. Machacek, M.I.K. Santala, I. Watts, P.A. Norreys, A.E. Dangor, Phys. Rev. Lett. **85**, 1654 (2000)

16 T. Ditmire, J.W.G. Tisch, E. Springate, M.B. Mason, R.A. Smith, J. Marangoos, M.H.R. Hutchinson, Nature **386**, 54 (1997); J. Jha, D. Mathur, M. Krishnamurthy, Appl. Phys. Lett. **88**, 41 107 (2006)
17 S. Ter-Avetisyan, M. Schnurer, S. Busch, E. Risse, P.V. Nickles, W. Sandner, Phys. Rev. Lett. **93**, 155 006 (2004)
18 P.P. Rajeev, P. Taneja, P. Ayyub, A.S. Sandhu, G.R. Kumar, Phys. Rev. Lett. **90**, 115 002 (2003)
19 J. Gersten, A. Nitzan, J. Chem. Phys. **73**, 3023 (1980)
20 P.F. Liao, A. Wokaun, J. Chem. Phys. **76**, 751 (1982)
21 P.P. Rajeev, P. Ayyub, S. Bagchi, G.R. Kumar, Opt. Lett. **29**, 2662 (2004)
22 P. Ayyub, R. Chandra, P. Taneja, A.K. Sharma, R. Pinto, Appl. Phys. A **73**, 67 (2001)
23 J.F. Ziegler, Nucl. Instrum. Methods Phys. Res. B **219–220**, 1027 (2004)
24 CASINO 2.0, http://www.gel.usherbrooke.ca/casino/index.html
25 D.W. Forslund, J.M. Kindel, K. Lee, Phys. Rev. Lett. **39**, 284 (1977)
26 R.A. Cairns, Plasma Phys. **20**, 991 (1978)
27 J.J. Thomson, C.E. Max, J. Erkkila, J.E. Tull, Phys. Rev. Lett. **37**, 1052 (1976)
28 G. Kulcsár, D. AlMawlawi, F.W. Budnik, P.R. Herman, M. Moskovits, L. Zhao, R.S. Marjoribanks, Phys. Rev. Lett. **84**, 5149 (2000)
29 P.P. Rajeev, S. Kahaly, S. Bagchi, S. Bose, P.P. Kiran, P. Taneja, P. Ayyub, G.R. Kumar, J. Phys. IV France **133**, 533 (2006)
30 A.J. Kemp, H. Ruhl, Phys. Plasmas **12**, 33 105 (2005)
31 V.Y. Bychenkov, V.N. Novikov, D. Batani, V.T. Tikhonchuk, S.G. Bochkarev, Phys. Plasmas **11**, 3242 (2004)
32 X. Wang, K. Nemoto, T. Naguki, Y. Oishi, K. Eidman, Phys. Plasmas **12**, 11 301 (2005)
33 M. Kaluza, J. Schrieber, M.I.K. Santala, G.D. Tsakiris, K. Eidman, J. Meyer-ter-Vehn, K.J. White, Phys. Rev. Lett. **93**, 045 006 (2004)
34 P.A. VanRompay, M. Nantel, P.P. Pronko, Surf. Coat. Technol. **100–101**, 496 (1998)
35 F. Amiranoff, R. Fedosejevs, R.F. Schmalz, R. Sigel, Y. Tung, Phys. Rev. A **32**, 3535 (1985)
36 M. Roth, A. Blazevic, M. Geissel, T. Schlegel, T.E. Cowan, M. Allen, J.C. Gauthier, P. Audebert, F. Fuchs, J. Meyer-ter-Vehn, M. Hegelich, S. Karsch, A. Pukhov, Phys. Rev. ST Accel. Beams **5**, 061 301 (2002)
37 A.J. Mackinnon, M. Borghesi, S. Hatchett, M.H. Key, P.K. Patel, H. Campbell, A. Schiavi, R. Snavley, S.C. Wilks, O. Willi, Phys. Rev. Lett. **86**, 1769 (2001)
38 Y. Tao, M.S. Tillack, Appl. Phys. Lett. **89**, 111 502 (2006)
39 H.A. Sumeruk, S. Kniep, D.R. Symes, I.V. Churina, A.V. Belolipeski, T.D. Donnely, T. Ditmire, Phys. Rev. Lett. **98**, 045 001 (2007)